

## Triaxial Projected Shell Model Approach

J. A. Sheikh<sup>1,2,3</sup> and K. Hara<sup>1</sup>

<sup>1</sup>*Physik-Department, Technische Universität München, D-85747 Garching, Germany*

<sup>2</sup>*Institut de Recherches Subatomiques (IReS), Université Louis Pasteur, 23 rue du Loess, F-67037 Strasbourg Cedex 2, France*

<sup>3</sup>*Tata Institute of Fundamental Research, Colaba, Bombay 400 005, India*

(Received 21 December 1998)

The projected shell model analysis is carried out using the triaxial Nilsson + BCS basis. It is demonstrated that, for a better description of the moments of inertia of nuclei in the transitional region, it is necessary to take the triaxiality into account and perform the three-dimensional angular momentum projection from the triaxial Nilsson + BCS intrinsic wave function. [S0031-9007(99)09068-7]

PACS numbers: 21.60.Cs, 21.10.Hw, 21.10.Ky, 27.70.+q

The major advancement in the studies of deformed nuclei has been the introduction of the Nilsson potential [1]. It was shown that the rotational properties of deformed nuclei can be described by considering nucleons to move in a deformed potential. The description of medium and heavy deformed nuclei in terms of the standard (spherical) shell model is almost impossible despite the recent progress in the computer technology. The Nilsson model has provided a useful nomenclature for the observed rotational bands adjusted to the proper shell filling of the individual nucleus. The Nilsson or deformed state is defined in the intrinsic frame of reference in which the rotational symmetry has been broken so that, in order to calculate the observable properties, it is necessary to restore the broken rotational symmetry, which can be done by using the standard angular momentum projection operator [2]. This method has been used to project out the good angular momentum states from the Nilsson + BCS intrinsic state [3–6]; see also the review article [7] and references cited therein. In this approach, the angular momentum projection is carried out from a chosen set of Nilsson + BCS states near the Fermi energy. The projected states are then used to diagonalize a shell model Hamiltonian. This approach, referred to as the projected shell model (PSM), follows the basic philosophy of the standard shell model approach. The only difference is that, in the PSM, the deformed basis is employed rather than the spherical one. This makes the truncation of the many-body basis very efficient, so that the shell model calculations even for heavier systems can be easily performed.

The PSM approach has been used to describe a broad range of nuclear phenomena such as backbending [8], signature dependence [9,10], superdeformed [11,12], and identical bands [13] with a considerable success. So far, the assumption in the PSM approach has been the axial symmetry for the deformed system to keep the computation simple. In fact, this is a reasonable assumption for well-deformed nuclei. However, for transitional nuclei, its validity is questionable. The inadequacy of the axially symmetric basis can be clearly demonstrated by moments

of inertia (the backbending plots) of the transitional nuclei in the rare-earth region. It has been shown [7] that, in the low spin region (i.e., spin not greater than 10), observed moments of inertia for lighter rare-earth nuclei (for instance, <sup>156</sup>Er, <sup>158</sup>Er, <sup>158</sup>Yb, and <sup>162</sup>Hf) and for the heavier rare-earth (for instance, <sup>172</sup>W, <sup>174</sup>W, and <sup>176</sup>W) increase quite steeply with increasing rotational frequency as compared to the moment of inertia calculated by the axially symmetric PSM approach (see Figs. 14–17 in [7]). This can be easily understood if one notes that the horizontal (vertical) line in the backbending plot represents the rotational (vibrational) limit since the energy  $E^I$  as a function of spin  $I$  behaves proportional to  $I^2$  ( $I$ ). In this sense, the experimental data slant towards the vibrational side in comparison with the axial PSM results. On the other hand, the spectrum of a triaxial rotor [14] is known to vary from rotational spectrum to a vibrational one as the triaxiality parameter  $\gamma$  increases from  $0^\circ$  to  $30^\circ$  and, using this model, it has been demonstrated (see Fig. 18 in [7]) that the backbending plot indeed approaches towards the vibrational limit when  $\gamma$  is made larger. It is therefore expected that the moments of inertia and other properties of the transitional nuclei may be described more accurately by using the triaxial basis in the PSM. As pointed out in [7], the major problem here lies rather in the ground state band. This part of the spectrum is quite insensitive to the configuration mixing since the spin (and energy) values are still low ( $I < 10$ ), so that an improvement of the ground band can be done only by allowing some triaxiality. The purpose of the present work is to develop a triaxial projected shell model (referred to as TPSM hereafter) for the description of transitional nuclei. This requires a three-dimensional angular momentum projection which has not been so intensively studied till now except for two investigations in the early eighties [15,16]. We have taken up this problem once again from a different point of view. The necessity of triaxiality will be demonstrated by comparing the numerical results with experimental data.

The shell model Hamiltonian employed in the present work is the same as the one used in the axially symmetric PSM approach [7]. This will make the difference

of the present approach to the earlier (axial) PSM particularly clear. It consists of  $Q \cdot Q$  + monopole pairing + quadrupole pairing forces,

$$\hat{H} = \hat{H}_0 - \frac{\chi}{2} \sum_{\mu} \hat{Q}_{\mu}^{\dagger} \hat{Q}_{\mu} - G_M \hat{P}^{\dagger} \hat{P} - G_Q \sum_{\mu} \hat{P}_{\mu}^{\dagger} \hat{P}_{\mu}. \quad (1)$$

Here,  $\hat{H}_0$  is the spherical harmonic-oscillator single-particle Hamiltonian with a proper  $l \cdot s$  force while the operators  $\hat{Q}$  and  $\hat{P}$  are defined as

$$\begin{aligned} \hat{Q}_{\mu} &= \sum_{\alpha\beta} Q_{\mu\alpha\beta} c_{\alpha}^{\dagger} c_{\beta}, & \hat{P}^{\dagger} &= \frac{1}{2} \sum_{\alpha} c_{\alpha}^{\dagger} c_{\bar{\alpha}}^{\dagger}, \\ \hat{P}_{\mu}^{\dagger} &= \frac{1}{2} \sum_{\alpha\beta} Q_{\mu\alpha\beta} c_{\alpha}^{\dagger} c_{\beta}^{\dagger}, \end{aligned} \quad (2)$$

where the quadrupole matrix elements are given by

$$Q_{\mu\alpha\alpha'} = \delta_{NN'} (Njm | Q_{\mu} | N'j'm'). \quad (3)$$

Here,  $\alpha = \{Njm\}$  while  $\bar{\alpha}$  represents the time-reversed state of  $\alpha$ . The Hartree-Fock-Bogoliubov (HFB) approximation of the shell model Hamiltonian Eq. (1) leads to the quadrupole mean field which is similar to the Nilsson potential. Therefore, instead of performing the HFB variational analysis of the Hamiltonian in Eq. (1), the Nilsson potential can be directly used to obtain the deformed basis. In the present work, we use the triaxial Nilsson potential specified by the deformation parameters  $\epsilon$  and  $\epsilon'$ ,

$$\hat{H}_N = \hat{H}_0 - \frac{2}{3} \hbar\omega \left( \epsilon \hat{Q}_0 + \epsilon' \frac{\hat{Q}_{+2} + \hat{Q}_{-2}}{\sqrt{2}} \right), \quad (4)$$

to generate the deformed single-particle wave functions. The  $Q \cdot Q$  coupling constant is adjusted such that the input deformation parameter  $\epsilon$  should be equal to the one resulting from the HFB calculation [7]. It can be easily seen that the rotation operator  $e^{-i(\pi/2)\hat{J}_z}$  transforms the Nilsson Hamiltonian  $\hat{H}_N$  into the opposite triaxiality ( $\epsilon' \rightarrow -\epsilon'$ ) leaving the eigenvalues unchanged. It will be shown later that the projected energy is independent of the sign of  $\epsilon'$  so that it is sufficient to consider only the non-negative  $\epsilon'$ . The volume conservation also restricts the range of  $\epsilon$  and  $\epsilon'$  values to

$$-3 < \epsilon < \frac{3}{2}, \quad |\epsilon'| < \sqrt{3} \left( 1 + \frac{\epsilon}{3} \right). \quad (5)$$

The triaxial Nilsson potential has been solved for the rare-earth region with three major shells  $N = 4, 5, 6$  (3, 4, 5) for neutrons (protons).

In the next step, the monopole pairing Hamiltonian is treated based on the triaxial Nilsson basis. We use the standard strengths for the pairing interaction of the form

$$G_M = \left( G_1 \mp G_2 \frac{N-Z}{A} \right) \frac{1}{A}, \quad (6)$$

where  $-$  ( $+$ ) is the neutrons (protons) while  $G_1$  and  $G_2$  are chosen, respectively, as 21.24 and 13.86 MeV. The

strength of the quadrupole pairing is set to  $G_Q = 0.18G_M$ , which is the standard value used in the PSM. The (static) pairing correlations are treated by the usual BCS approximation to establish the Nilsson + BCS basis. The three-dimensional angular momentum projection is then carried out on the quasiparticle states obtained in this way.

The angular momentum projection operator is given by

$$\hat{P}_{MK}^I = \frac{2I+1}{16\pi^2} \int d\Omega D_{MK}^I(\Omega) \hat{R}(\Omega), \quad (7)$$

with  $\hat{R}(\Omega) = e^{-i\alpha\hat{J}_z} e^{-i\beta\hat{J}_y} e^{-i\gamma\hat{J}_z}$  being the rotation operator and  $D_{MK}^I(\Omega) = \langle \nu IM | \hat{R}(\Omega) | \nu IK \rangle^*$  its irreducible representation, where  $\{|\nu IM\rangle\}$  is a complete set of states for the specified angular momentum quantum number  $IM$ . Since the spectral representation of the projection operator Eq. (7) is represented by

$$\hat{P}_{MK}^I = \sum_{\nu} |\nu IM\rangle \langle \nu IK|, \quad (8)$$

it is easy to see that  $|\Phi'\rangle \equiv e^{-i(\pi/2)\hat{J}_z} |\Phi\rangle$ , i.e., the state of the opposite triaxiality to a state  $|\Phi\rangle$ , is projected to give

$$\hat{P}_{MK}^I |\Phi'\rangle = \hat{P}_{MK}^I e^{-i(\pi/2)\hat{J}_z} |\Phi\rangle = (-)^{-i(\pi/2)K} \hat{P}_{MK}^I |\Phi\rangle. \quad (9)$$

This state differs only by a phase factor from  $\hat{P}_{MK}^I |\Phi\rangle$  and thus represents the same physical state. It therefore proves that the result of the angular momentum projection should be independent of the sign of  $\epsilon'$ . We have used this property to check the programming since it is a nontrivial relation. Note that this justifies the above-mentioned restriction  $\epsilon' \geq 0$ . Details of the projection technique and algorithm are discussed in Appendix A of Ref. [7].

In the present work, we have diagonalized the Hamiltonian Eq. (1) within the space spanned by  $\{\hat{P}_{MK}^I |\Phi\rangle\}$  where  $|\Phi\rangle$  is the (triaxial) quasiparticle vacuum state. The TPSM eigenvalue equation with the eigenvalue  $E^I$  for a given spin  $I$  thus becomes

$$\sum_{K'} (H_{KK'}^I - E^I N_{KK'}^I) F_{K'}^I = 0, \quad (10)$$

where the matrix elements are defined by

$$H_{KK'}^I = \langle \Phi | \hat{H} \hat{P}_{KK'}^I | \Phi \rangle, \quad N_{KK'}^I = \langle \Phi | \hat{P}_{KK'}^I | \Phi \rangle. \quad (11)$$

This TPSM equation has been solved for several nuclei in the rare-earth region up to  $I = 10$ , below which the 2- and higher-quasiparticle bands would be less important. The results of a selected few are presented in Figs. 1 and 2.

The deformation parameters  $\epsilon$  used in Fig. 1 are exactly the same as those used in the earlier calculations with the axially symmetric basis [7], i.e.,  $\epsilon = 0.20, 0.20, \text{ and } 0.225$  for  $^{156}\text{Er}$ ,  $^{158}\text{Yb}$ , and  $^{176}\text{W}$ , respectively. Therefore, the results with  $\epsilon' = 0.0$  in Fig. 1 correspond to the earlier axially symmetric calculations. Note that the experimental moments of inertia (represented by circles

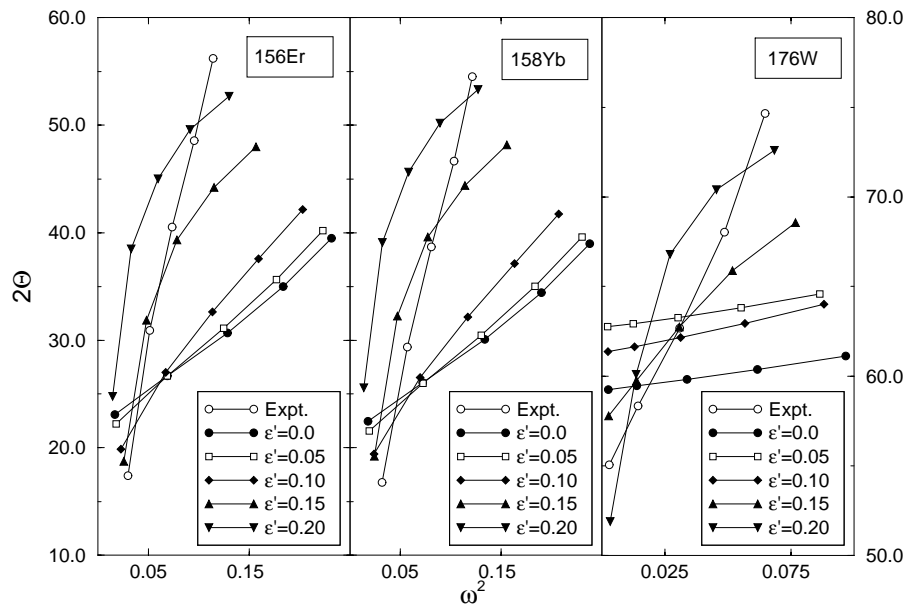


FIG. 1. The experimental and the calculated moments of inertia ( $\Theta$ ) are plotted as a function of the rotational frequency ( $\omega$ ) for  $^{156}\text{Er}$ ,  $^{158}\text{Yb}$ , and  $^{176}\text{W}$ . It is clearly seen that the experimental moments of inertia are reproduced with the triaxiality  $\epsilon' \approx 0.15$  for all three cases.

in the figures) increase quite steeply. The calculations with  $\epsilon' = 0.0$ , on the other hand, depict a very slow increase and is typical of an axially deformed rotational band. The moments of inertia in Fig. 1 become steeper with the increasing value of  $\epsilon'$  and the value close to  $\epsilon' = 0.15$  reproduces the experimental data. Roughly speaking, this  $\epsilon'$  value corresponds to  $\gamma = 35^\circ$ . It should be noted that the experimental moment of inertia shown

in Fig. 1 slightly increases, in particular, for  $^{176}\text{W}$ , at the higher end, whereas the theoretical moment of inertia shows a drop. This increase in the observed moment of inertia can be explained by the fact that, at around spin  $I = 12^+$ , a 2-quasiparticle band (i.e., the  $s$  band) will cross with the ground band and the energy of the higher spin states will thus be depressed, so that the moment of inertia will effectively increase. In the present

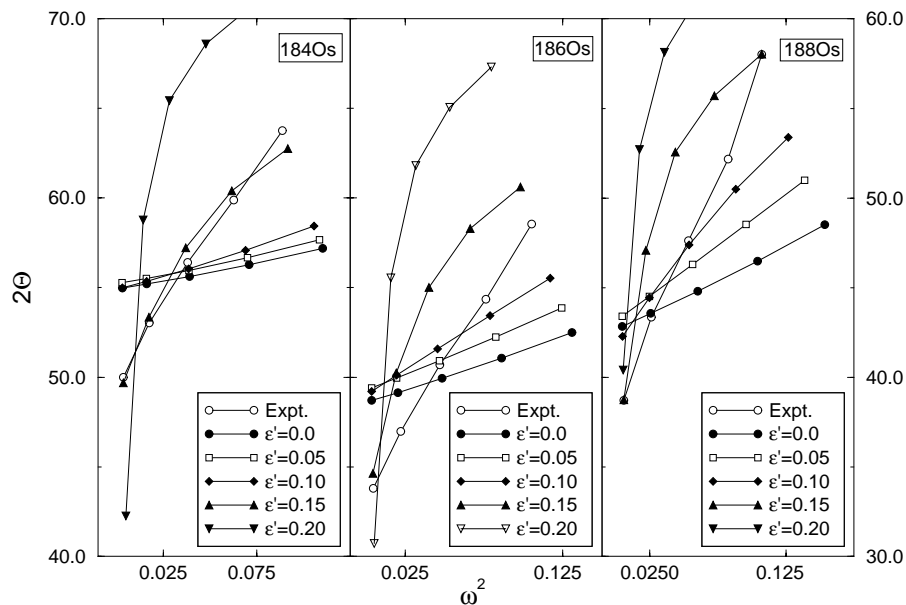


FIG. 2. The experimental and the calculated moments of inertia ( $\Theta$ ) are plotted as a function of the rotational frequency ( $\omega$ ) for  $^{184}\text{Os}$ ,  $^{186}\text{Os}$ , and  $^{188}\text{Os}$ . For  $^{184}\text{Os}$ , the experimental moment of inertia is very well reproduced with  $\epsilon' \approx 0.15$ . For  $^{186}\text{Os}$  and  $^{188}\text{Os}$ , it can be described with  $\epsilon'$  between 0.10 and 0.15.

calculations, the projection has been carried out only from the ground (i.e., the 0-quasiparticle) band and this effect is not taken into account. The projection from 2- and higher-quasiparticle states requires further work and will be reported elsewhere.

In a similar fashion, Fig. 2 shows the moments of inertia for some Os isotopes. It is known that these isotopes are  $\gamma$  soft with very low-lying  $\gamma$  bands. A study of the  $\gamma$  bands will be reported elsewhere. It is clear from Fig. 2 that, for  $^{184}\text{Os}$ , the moment of inertia is well reproduced with  $\epsilon' = 0.15$ . For  $^{186}\text{Os}$  and  $^{188}\text{Os}$ , the experimental moment of inertia can be explained with  $\epsilon'$  between 0.10 and 0.15.

In summary, it has been clearly shown in the present work that the three-dimensional angular momentum projection from a triaxial Nilsson + BCS deformed intrinsic wave function is essential for a better description of the transitional nuclei. The moments of inertia of these nuclei depict a steep increase as functions of the rotational frequency in the low spin region ( $I < 10$ ) and this can be explained only with a triaxial deformation of  $\gamma \simeq 30^\circ$  since the inclusion of the 2- and higher-quasiparticle bands will contribute little in this low spin (and low excitation energy) region.

The present work is of a preliminary nature. For a detailed study, the projected energy surface has to be analyzed as a function of  $\epsilon$  and  $\epsilon'$  to look for the optimal deformation. In the present work, the deformation parameter  $\epsilon$  has been taken from the earlier studies in which the axial symmetry was assumed. In a more consistent treatment, both  $\epsilon$  and  $\epsilon'$  have to be varied in order to search the minimum of the ground state energy [16], although it is not obvious whether or not a schematic

Hamiltonian such as the present one ( $Q \cdot Q$  + monopole pairing + quadrupole pairing force model) can correctly describe the problem associated with the absolute (ground state) energy. In contrast to this, the relative (excitation) energies are insensitive to details of the Hamiltonian and can thus be described rather reliably as proved in Appendix B of Ref. [7]. At the moment, we are working on the electromagnetic properties to study the effect of triaxiality on the transitions. This will be reported elsewhere.

- 
- [1] S. G. Nilsson, Dan. Mat. Fys. Medd. **29**, 16 (1955).
  - [2] P. Ring and P. Schuck, *The Nuclear Many-Body Problem* (Springer-Verlag, Heidelberg, New York, 1980).
  - [3] K. Hara and S. Iwasaki, Nucl. Phys. **A332**, 61 (1979).
  - [4] K. Hara and S. Iwasaki, Nucl. Phys. **A348**, 200 (1980).
  - [5] S. Iwasaki and K. Hara, Prog. Theor. Phys. **68**, 1782 (1982).
  - [6] K. Hara and S. Iwasaki, Nucl. Phys. **A430**, 175 (1984).
  - [7] K. Hara and Y. Sun, Int. J. Mod. Phys. **E4**, 637 (1995).
  - [8] K. Hara and Y. Sun, Nucl. Phys. **A529**, 445 (1991).
  - [9] K. Hara and Y. Sun, Nucl. Phys. **A531**, 221 (1991).
  - [10] K. Hara and Y. Sun, Nucl. Phys. **A537**, 77 (1992).
  - [11] Y. Sun and M. Guidry, Phys. Rev. C **52**, R2844 (1995).
  - [12] Y. Sun, J.-y. Zhang, and M. Guidry, Phys. Rev. Lett. **78**, 2321 (1997).
  - [13] Y. Sun, C.-L. Wu, D. H. Feng, J. L. Egido, and M. Guidry, Phys. Rev. C **53**, 2227 (1996).
  - [14] A. S. Davydov and F. G. Filippov, Nucl. Phys. **8**, 237 (1958).
  - [15] K. Hara, A. Hayashi, and P. Ring, Nucl. Phys. **A385**, 14 (1982).
  - [16] A. Hayashi, K. Hara, and P. Ring, Phys. Rev. Lett. **53**, 337 (1984).